Correspondence

High-Frame-Rate Echocardiography With Reduced Sidelobe Level

Hideyuki Hasegawa and Hiroshi Kanai

Abstract—**Echocardiography has become an indispensable modality for diagnosis of the heart. It enables observation of the shape of the heart and estimation of global heart function based on B-mode and M-mode imaging. Methods for echocardiographic estimation of myocardial strain and strain rate have also been developed to evaluate regional heart function. Furthermore, it has been recently shown that echocardiographic measurements of transmural transition of myocardial contraction/relaxation and propagation of vibration caused by closure of the heart valve would be useful for evaluation of myocardial function and viscoelasticity. However, such measurements require a frame rate (typically >200 Hz) much higher than that achieved by conventional ultrasonic diagnostic equipment. We have recently realized a high frame rate of about 300 Hz with a full field of view of 90° using diverging transmit beams and parallel receive beamforming. Although high-frame-rate imaging was made possible by this method, the side lobe level was slightly larger than that of the conventional method. To reduce the side lobe level, phase coherence imaging has recently been developed. Using this method, the spatial resolution is improved and the side lobe level is also reduced. However, speckle-like echoes, for example, echoes from the inside of the heart wall, are also suppressed. In the present study, a method for reducing the side lobe level while preserving speckle-like echoes was developed. The side lobe level was evaluated using a wire phantom. The side lobe level of the high-frame-rate imaging using unfocused diverging beams was improved by 13.3 dB by the proposed method. In *in vivo* measurements, a B-mode image of the heart of a 23-year-old healthy male could be obtained while preserving the speckle pattern in the heart wall at a frame rate of 316 Hz with a full field of view of 90°.**

I. Introduction

Echocardiography is a predominant modality for diagnosis of the heart because it provides a cross-sectional image of the heart noninvasively in real time. Because of the high temporal resolution of ultrasonic diagnostic equipment, global heart function, such as ejection fraction (EF), can be estimated based on B-mode and M-mode imaging much more easily than with other diagnostic modalities, such as magnetic resonance imaging (MRI) and computed tomography (CT). It has recently been shown that ultrasonic measurements of transmural transition of myocardial contraction/relaxation and its propagation [1], [2] and propagation of vibration caused by closure of a heart valve would be useful for evaluation of myocardial function and viscoelasticity [3], [4]. However, such measurements require a frame rate much higher than that achieved by conventional ultrasonic diagnostic equipment. For example, electrical excitation propagates in Purkinje fibers and ventricular muscle at typical velocities of 0.3 to 4 m/s [5], and the corresponding propagation velocities of myocardial contraction of 0.5 to 7 m/s have been measured by ultrasound [4], [6]. In these studies, a high frame rate (typically higher than 400 Hz with a slightly reduced lateral field of view, which is much higher than that realized by conventional ultrasonic diagnostic equipment, usually several tens of hertz) is required to measure the propagation of this electromechanical wave and the resulting transient small motion of the heart wall.

Konofagou *et al.* [7] and D'hooge *et al.* [8] increased the frame rate to above 200 Hz in the ultrasonic measurement of the heart function. However, the size of the field of view and the total number of scan lines in an ultrasonic image were significantly reduced.

To achieve a high frame rate, we used sparse sector scanning, in which the number of scan lines was decreased to about 10 [9], and applied it to various applications [1]–[4]. In this method, the angle intervals between scan lines are increased to obtain a large lateral field of view with a small number of scan lines. Therefore, the lateral image resolution is significantly degraded.

The aforementioned methods are based on conventional beamforming; therefore, the density of scan lines or field of view must be sacrificed to achieve a high frame rate. To overcome this problem, parallel receive beamforming [10] with a wide transmit beam has been developed to illuminate a wider region by one transmission to reduce the number of transmissions. Lu and colleagues proposed an imaging method using an unfocused but nondiverging transmit beam, namely, a limited diffraction beam [11]–[14]. Unfocused beams achieved a wider beam width, and nondiverging beams used in these cited studies prevented the insonified energy from being spread to ensure that the required penetration depth was achieved. However, the width of a nondiverging beam is limited by the size of the aperture, which would limit the number of receiving beams created by one transmission.

High-frame-rate echocardiography at about 300 Hz with a full field of view of 90° using steered diverging transmit beams and parallel receive beamforming has recently been realized [15]. Diverging waves were produced using all transducer elements in an ultrasonic array probe to obtain ultrasonic echoes with a better SNR [16], [17] than the spherical wave produced by a single element [18]. Although just the idea of a diverging beam produced from multiple elements was shown in [17], the feasibility of the diverging beam had not been examined. The diverging beam from multiple elements was shown to be feasible in high-frame-rate echocardiography [15]. Although high-frame-rate imaging is possible by our method, the side lobe

Manuscript received December 20, 2011; accepted July 20, 2012.

The authors are with the Graduate School of Biomedical Engineering and the Graduate School of Engineering, Tohoku University, Sendai, Japan (e-mail: hasegawa@ecei.tohoku.ac.jp).

DOI http://dx.doi.org/10.1109/TUFFC.2012.2490

level is slightly larger than that of conventional beamforming. To reduce the side lobe level, phase coherence imaging has recently been developed [19]. This method sensitively suppresses echoes influenced by the diversity of phases of echoes received by transducer elements because of various factors, such as focusing error, etc. Therefore, the spatial resolution is improved and the side lobe level is suppressed by this method, but weak speckle-like echoes, which are generated by interference of scattered echoes, are also significantly suppressed because the phases of echoes would be influenced by the interference. In the present study, a method to reduce the side lobe level while preserving speckle-like echoes was developed. The side lobe level was evaluated using a wire phantom, and a B-mode image of a heart of a 23-year-old healthy male was obtained *in vivo* by the proposed method.

II. Principles

Using an unfocused wide transmit beam increases the side lobe level compared with conventional beamforming (focusing both in transmit and receive). Therefore, methods for reduction of the side lobe level are required.

When receive focusing is performed with respect to a spatial point $\mathbf{p}$, the position of the source of an echo does not always exactly coincide with $\mathbf{p}$. Let us consider the difference between the time delay applied by a receive beamformer and the propagation time delay of the echo. As shown in Fig. 1(a), the locations of focus and the source of the echo are defined by (x, z) and $(x + \Delta x, z + \Delta z)$, respectively. Under such conditions, distance r_i' from the ith element to the source and distance r_i from the ith element to the focal point are expressed as

$$r_i' = \sqrt{(x - x_i + \Delta x)^2 + (z + \Delta z)^2}, \tag{1}$$

$$r_i = \sqrt{(x - x_i)^2 + z^2}, \tag{2}$$

where x_i is the lateral position of the ith element.

Residual time delay $\Delta\tau_i$ (focusing error) of the echo from the source received by the ith element after receive beamforming (applying time delay $T_{\mathrm{RBF},i}$) depends on the difference between r_i and r_i'.

$$\begin{aligned}(r_i')^2 - r_i^2 &= \Delta r_i(2r_i + \Delta r_i) \\ &= (x - x_i + \Delta x)^2 + (z + \Delta z)^2 - (x - x_i)^2 - z^2,\end{aligned} \tag{3}$$

where Δr_i is $r_i' - r_i$.

By assuming that the focal depth z is sufficiently large, squares of Δx and Δz can be neglected:

$$\Delta r_i(2r_i + \Delta r_i) \approx 2\Delta x(x - x_i) + 2\Delta z \cdot z, \tag{4}$$

$$\begin{aligned}\Delta r_i &= \frac{2\Delta x(x - x_i) + 2\Delta z \cdot z}{2r_i + \Delta r_i} \\ &\approx \frac{\Delta x(x - x_i) + \Delta z \cdot z}{r_i},\end{aligned} \tag{5}$$

where $2r_i + \Delta r_i$ is approximated by $2r_i$ because Δr_i is assumed to be sufficiently smaller than $2r_i$.

For large z, distance r_i can be approximated to be $(x^2 + z^2)^{1/2}$ because x_i is limited by the aperture size (x_i was less than 10 mm in the present study). Therefore, residual time delay $\Delta\tau_i$ is expressed as

$$\begin{aligned}\Delta\tau_i &= \frac{\Delta r_i}{c_0} \\ &\approx ax_i + b,\end{aligned} \tag{6}$$

where c_0 is the speed of sound. Constants a and b are given by

$$a = \frac{\Delta x}{c_0\sqrt{x^2 + z^2}}, \tag{7}$$

$$b = \frac{\Delta x \cdot x + \Delta z \cdot z}{c_0\sqrt{x^2 + z^2}}. \tag{8}$$

Residual time delay $\Delta\tau_i$ is also expressed as the residual phase delay $\Delta\theta_i$:

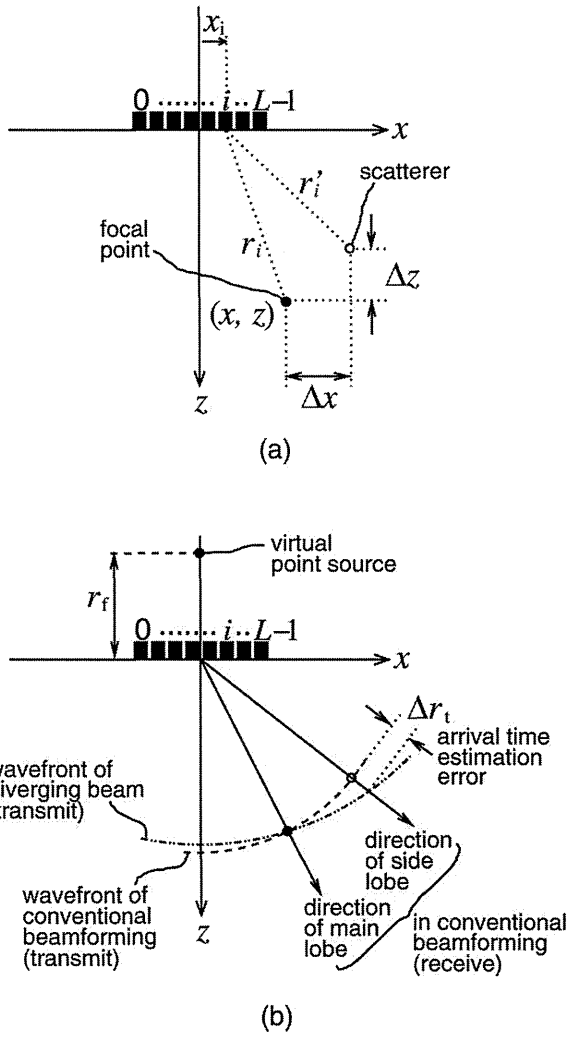

Fig. 1. Illustration of mismatch between the location of a focal point and that of the source of an echo (a) in receive and (b) in transmission.

$$\Delta\theta_i = 2\pi f_0 \Delta\tau_i, \tag{9}$$

where f_0 is the center frequency of ultrasound. In the present study, a method was proposed for reduction of the side lobe level while keeping the shape of the point spread function similar to those in conventional beamforming and our proposed method using diverging beams. As shown in (6), there is a linear relationship between the residual phase delay $\Delta\theta_i$ and the lateral position x_i of an element when the location of a focal point is close to that of a scatterer. This means that the difference between residual phase delays of two neighboring elements is consistent across the array when the focusing is done near the source of an echo (when Δx and Δz are small). This consistency can be evaluated by the magnitude-squared coherence function (MSCF) γ [20], defined as:

$$\gamma = \frac{\left|\sum_{i=0}^{L-2} S_i^* \cdot S_{i+1}\right|^2}{\sum_{i=0}^{L-2}|S_i|^2 \sum_{i=0}^{L-2}|S_{i+1}|^2}, \tag{10}$$

where L is the number of elements. The numerator in (10) corresponds to the cross-spectrum between S_i and S_{i+1} averaged across the array. Therefore, the MSCF becomes 1 when the transfer function from S_i to S_{i+1} is constant across the array. On the other hand, the magnitude of the numerator decreases because of the incoherent averaging of the transfer function when the transfer function is not constant. The phase of the transfer function corresponds to the phase difference between two neighboring elements. Therefore, the MSCF would decrease when the phase difference between two neighboring elements is not constant [= nonlinear according to the element number (position)].

To obtain the MSCF γ, the complex Fourier coefficient S_i' at f_0 (= 3.75 MHz) of the RF echo signal $s_i(t - T_{\mathrm{RBF},i})$ received by the ith transducer element must be estimated. To obtain the complex Fourier coefficient S_i', in the present study, the discrete Fourier transform at f_0 was applied to $s_i(t - T_{\mathrm{RBF},i})$ with a Hann window whose length was 0.53 μs. Under this condition, the first nulls of the power spectrum of the Hann window were located at 0 and 7.5 MHz, providing the available maximum bandwidth of the resultant complex signal S_i sampled at 30 MHz.

The Fourier transform was applied to the RF echo $s_i(t - T_{\mathrm{RBF},i})$ received by the ith transducer element after the time shift by the receiving beamformer to account for the differences among propagation time delays of echoes received by transducer elements. However, the time delay $T_{\mathrm{RBF},i}$ is an integral multiple of the sampling interval of the RF echo. To remove the residual time delay resulting from the difference between the actual time delay $\Delta\tau_i$ and $T_{\mathrm{RBF},i}$, S_i' is multiplied by $\exp\{2\pi f_0(\Delta\tau_i - T_{\mathrm{RBF},i})\}$ to obtain the corrected Fourier coefficient S_i in (10). Therefore, there are no phase differences among corrected Fourier coefficients $\{S_i\}$ when the location of the source of the echo exactly coincides with the focal point $\mathbf{p}$ [the relationship between residual time delay and an element's lateral position is linear, but both a and b in (6) are zero]. In this case, the MSCF γ is 1. In addition, according to (6) and (9), there is a linear relationship between the phase delay $\Delta\theta_i = \angle S_i$ and the lateral position x_i of the transducer element when the focal point is located very near the source of the echoes (small Δx and Δz). In such cases, the MSCF γ is also close to 1 because the phase difference between the spectra of the signals received by ith and $(i+1)$th elements is consistent across the array. On the other hand, the MSCF γ decreases when there is a mismatch between the locations of the source of an echo and the focal point, (e.g., echoes caused by side lobes) because the assumption of (4) is not applicable. Therefore, such undesirable echoes can be suppressed by weighting the beamformed RF signal at $\mathbf{p}$ using the MSCF γ.

Furthermore, the difference between transmit beams in conventional and proposed beamforming is considered to affect the side lobe reduction. In conventional beamforming, the geometrical center (center of the aperture) is same in both transmit and receive, as illustrated in Fig. 1(b). Therefore, the time required for the propagation of ultrasound from the aperture to a scatterer (in transmit) and that from the scatterer to the aperture (in receive) are same, and an echo from a scatterer, which is located at the range distance along the side lobe that is same as the range distance of the focal point, would contribute to the calculation of the MSCF at the spatial point $\mathbf{p} = (x, z)$.

On the other hand, the time required for the propagation from the aperture to the scatterer and that from the scatterer to the aperture are different in our beamforming using diverging beams because the geometrical center of the transmit beam is the position of a virtual source of a diverging beam. The time required for the propagation of a diverging beam from the aperture to a scatterer can be estimated correctly when the scatterer is located at the focal point. However, there is an arrival-time estimation error $\Delta\tau_t$, which reduces the contribution of the echo from the scatterer to the calculation of the MSCF at the spatial point $\mathbf{p}$ (there is no echo signal in beamforming at $\mathbf{p}$ when $\Delta\tau_t$ is larger than the pulse duration of ultrasound) when the scatterer is not at the focal point. Such arrival-time estimation error would also reduce the coherence of the received signals.

III. Evaluation of Spatial Resolution and Side Lobe Level Using a Wire Phantom

In the present study, a commercial diagnostic ultrasonic system (α-10, Aloka, Tokyo, Japan) was used with a 3.75-MHz phased array probe. The phased array was composed of $L = 96$ elements at intervals of 0.2 mm. The elevation focal distance was fixed to be 70 mm. This system was modified so that all of the 96 elements can be excited simultaneously and RF echoes received by $L = 96$ individual elements could be acquired at a sampling frequency of 30 MHz and a 16-bit resolution for off-line processing (receive beamforming, compounding, etc.). In conventional beamforming, receive focusing was done with

respect to each discrete spatial point. The beamforming procedure in our high-frame-rate imaging is described in [15]. The Hann apodization was used for both conventional beamforming and our high-frame-rate imaging. In the beamforming procedure, a constant speed of sound of 1540 m/s was assumed.

In the basic experiment, fine nylon wires (diameter ≈100 μm) placed in water were used for evaluation of the spatial resolution. Figs. 2(a)–2(d) show B-mode images of the wires obtained by conventional beamforming and parallel beamforming with diverging beams at r_f = 100 mm without weighting, with weighting by the MSCF, and with weighting by the phase coherence factor [19], respectively, where r_f is the distance between the front surface of the array and the virtual point source behind the array for producing a diverging beam. The dynamic ranges of Figs. 2(a)–2(d) are 60 dB. For diverging beams, distance r_f was set at 100 mm. In Fig. 2, there is not much difference between the B-mode image obtained by conventional beamforming [Fig. 2(a)] and those obtained using diverging beams with [Fig. 2(b)] and without [Fig. 2(c)] weighting by the MSCF. The B-mode image obtained using diverging beams with weighting by the phase coherence factor [Fig. 2(d)] shows a significantly improved spatial resolution compared with the other images. In Fig. 2(d), the phase coherence factor is obtained as max[0,1 − σ/σ_0] [19], where σ is the standard deviation of phases of echoes received by individual elements and $\sigma_0 = \pi/3^{0.5}$. The standard deviation σ was evaluated after applying time delays by the receiving beamformer.

Fig. 3 shows the lateral profiles of the images [corresponding to point spread functions (PSF)] at the shallowest wire. The half-full-widths at half-maxima of the point spread functions shown in Fig. 3 are provided in Table I. From the data shown in Fig. 3, the average side lobe levels were evaluated in the lateral angular ranges, −45° < (lateral angle) < −15° and 15° < (lateral angle) < 45°. The side lobe level obtained using diverging beams increased by 8.5 dB compared with conventional beamforming. By weighting with the MSCF, the side lobe level in the high-frame-rate imaging using diverging beams was reduced by 13.3 dB. Weighting by the phase coherence factor showed the best spatial resolution and the lowest side lobe level in the phantom experiment.

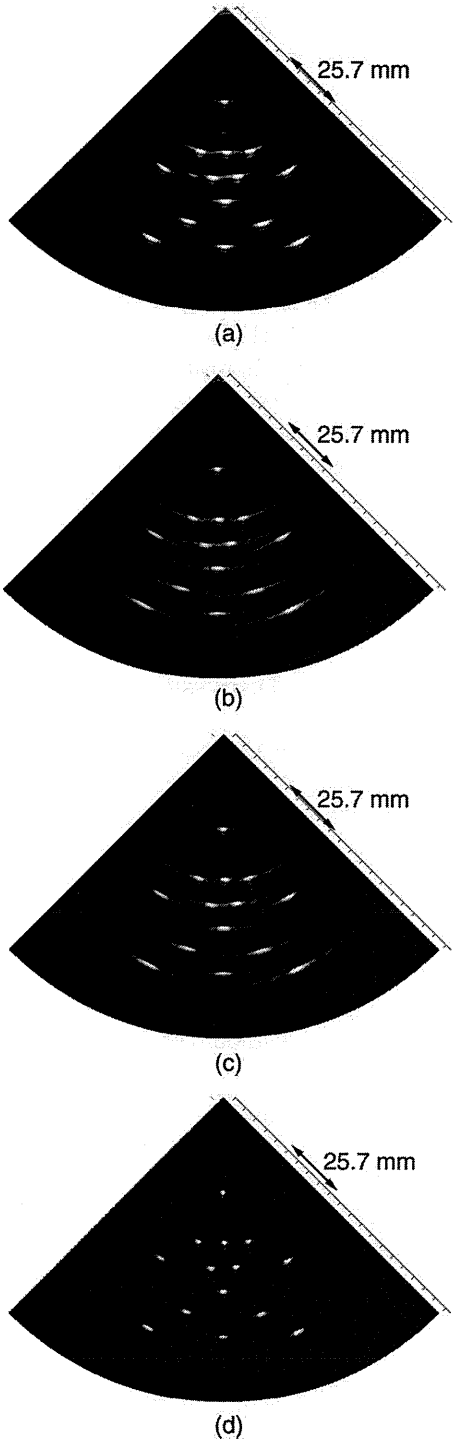

Fig. 2. B-mode images of fine wires obtained (a) by conventional sector scanning, (b) using a diverging beam, (c) using a diverging beam with weighting by the magnitude-squared coherence function (MSCF), and (d) using a diverging beam with phase coherence factor weighting [19].

IV. *In Vivo* Imaging of a Human Heart

Figs. 4(a)–4(d) show B-mode images of the heart of a 23-year-old healthy male obtained by conventional beamforming and parallel beamforming with diverging waves at r_f = 100 without weighting, with weighting by the MSCF, and with weighting by the phase coherence factor, respectively. Fig. 5 shows the intensity profiles along the scan lines indicated by the white lines in Fig. 4. Note that the position of the posterior wall in the measurement with conventional beamforming was slightly shallower than that in the measurement with diverging beams. Using diverging waves [Fig. 4(b)], a B-mode image of the heart could be obtained at a high frame rate of 316 Hz with a full lateral field of view of 90°. By weighting with the MSCF [Fig. 4(c)], the image contrast was improved, and speckle-like echoes, for example, echoes in the heart wall, were well preserved. It can be also observed in Fig. 5 that the proposed method using the MSCF suppresses the undesirable echoes in the cardiac lumen while keep-

TABLE I. HALF-FULL-WIDTHS AT HALF-MAXIMA OF POINT SPREAD FUNCTIONS SHOWN IN FIG. 3.

	Conventional beamforming	Diverging	Diverging with MSCF	Diverging phase coherence
Width of lateral PSF [mm]	0.66	0.82	0.81	0.43

ing the echoes inside the heart walls. On the other hand, by weighting with the phase coherence factor [Fig. 4(d)], speckle-like echoes inside the heart walls were significantly suppressed, although echoes resulting from specular reflection, such as an echo from the epicardium, were significantly enhanced. As shown in Fig. 3, although the spatial resolution is significantly improved by weighting with the phase coherence factor, this characteristic, i.e., significant suppression of speckle-like echoes, may not be preferable for analyzing the heart wall, such as estimation of velocity and strain rate of the heart wall.

V. DISCUSSION

Recently, we have developed a method based on parallel beamforming with diverging transmit beams for high-frame-rate echocardiography. To realize B-mode imaging in a sector format based on parallel beamforming, spherically diverging waves were used in transmission. However, in this method, the side lobe level slightly increased compared with that of conventional beamforming because of the use of unfocused transmit beams. In the present study, a method for reduction of side lobe level was developed to realize a side lobe level lower than that of conventional beamforming with a frame rate of over 300 Hz, which is much higher than that of conventional beamforming.

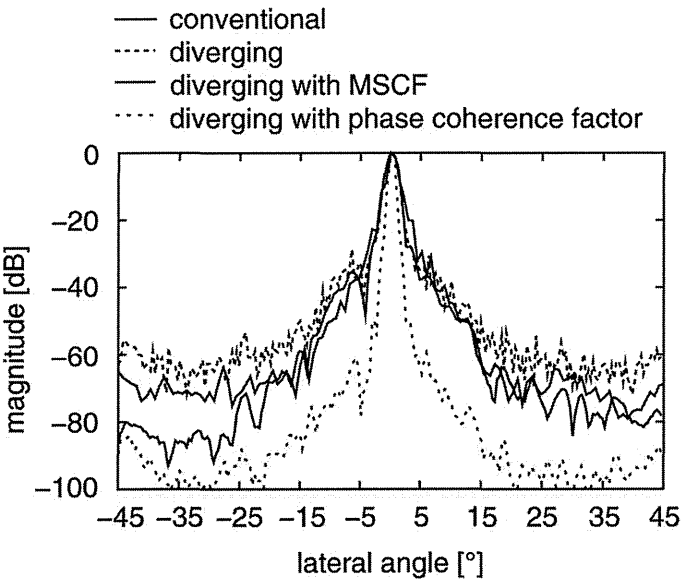

Fig. 3. Point spread functions in the lateral direction obtained by conventional sector scanning, diverging beam, diverging beam with weighting by the magnitude-squared coherence function (MSCF), and diverging beam with phase coherence factor weighting [19].

To consider small residual time delays of echoes, the phases of the echoes were used in the present study. To obtain the phase information, the Hilbert transform is used in general. However, the Hilbert transform requires the Fourier transform of the echo signal and the inverse Fourier transform of the estimated frequency spectrum. To increase the computational efficiency, in the present study, the Fourier coefficient of the echo at only the center frequency of ultrasound was calculated. This center frequency should be the center frequency of the received RF echo. However, in the present study, the center frequency of the ultrasound emitted was used because the estimation of the center frequency of the received echo required an additional computation. Before calculating the MSCF, time delays based on conventional focusing were applied to signals received by individual elements. In this procedure, sub-sample time delays were applied by considering the phase of the echo signal, as described in Section II. As expressed in (9), the phase delay coinciding with the corresponding time delay is expressed using the center frequency of the received echo. Therefore, there would be errors in application of time delays. However, such errors are negligible because the errors are smaller than the sampling interval of 25 ns.

In the results of imaging of wires, it was found that the side lobe reduction by the proposed method was depth-dependent, i.e., the side lobe reduction is smaller in a deeper region than a shallower region, because the change in the distance from a scatterer to an element caused by the lateral position of the element is smaller in a deeper region. As suggested for the phase coherence factor [19], the side lobe reduction can be controlled by taking γ^{α} (γ: MSCF), where α is a variable coefficient. Therefore, in our future work, it may be effective to control the weights by considering the depth-dependent characteristic of the MSCF γ.

To suppress the side lobe level, the phase coherence factor [19] was recently introduced. This method suppresses a beamformed echo signal whose standard deviation of phases of echoes received by transducer elements is large. Using this method, weak speckle-like echoes are also suppressed because the standard deviation of phases of echoes received by individual elements would be increased by interference of echoes, which is the source of speckle-like echoes. In some cases, it is important to observe speckle patterns of tissues. Therefore, a method for reduction of the side lobe level with preservation of speckle-like echoes was developed in the present study. On the other hand, the phase coherence factor improves spatial resolution and

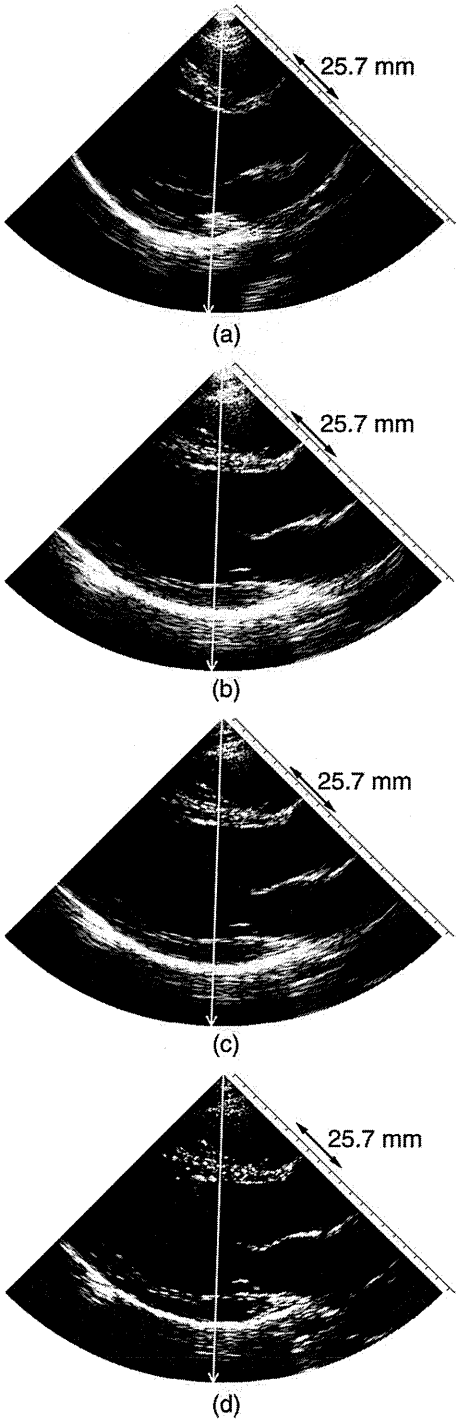

Fig. 4. B-mode images of the heart of a 23-year-old healthy male obtained (a) by conventional sector scanning, (b) using a diverging beam, (c) using a diverging beam with weighting by the magnitude-squared coherence function (MSCF), and (d) using a diverging beam with phase coherence factor weighting [19].

also well emphasizes specular echoes, such as echoes from heart valves in Fig. 4(d), and relatively strong scattering echoes. The method based on the phase coherence factor and the proposed method are complementary.

In high-frame-rate imaging, it is necessary to use unfocused transmit beams. Therefore, the side lobe level increases in general. Although optimization of transmit conditions, such as angular beam width, angular intervals

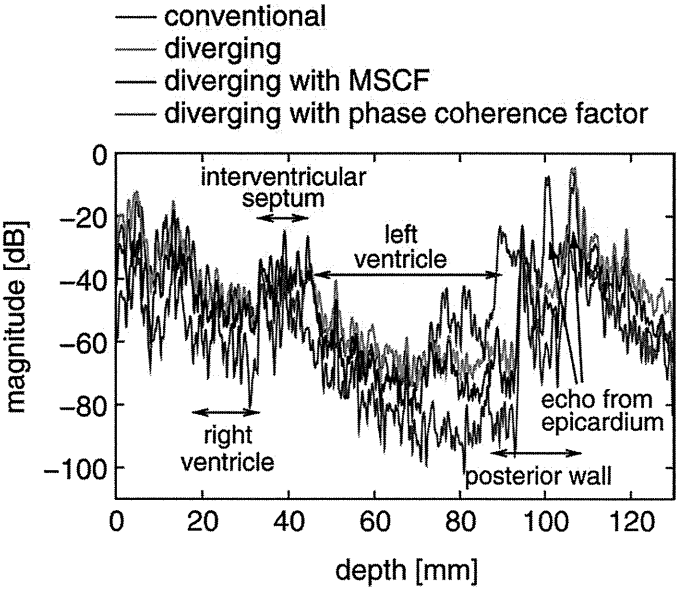

Fig. 5. Intensity profiles along the scan lines indicated by the white lines in Fig. 4.

of transmit beams, estimation of wavefronts of transmit beams, etc., are necessary to further improve the frame rate, such methods for reducing the side lobe level would be necessary for high-frame-rate imaging to obtain an image contrast comparable to or better than that obtained by conventional beamforming.

VI. Conclusions

In this study, a method of suppressing the side lobe level was developed for high-frame-rate echocardiography based on parallel beamforming with diverging transmit beams. To realize suppression of the side lobe level while preserving speckle-like echoes, the MSCF between echoes received by individual transducer elements was used for weighting a beamformed RF echo. Using the proposed method, it was confirmed by basic experiments using fine wires that the side lobe level could be reduced by 4.8 dB compared with conventional beamforming. Furthermore, in *in vivo* measurements, an ultrasonic image of a heart with a full field of view of 90° at a frame rate of 316 Hz could be obtained with an improved image contrast and preservation of speckle-like echoes.

References

[1] H. Kanai, "Propagation of vibration caused by electrical excitation in the normal human heart," *Ultrasound Med. Biol.*, vol. 35, no. 6, pp. 936–948, 2009.

[2] H. Kanai and M. Tanaka, "Minute mechanical-excitation wave-front propagation in human myocardial tissue," *Jpn. J. Appl. Phys.*, vol. 50, no. 7, art. no. 07HA01, 2011.

[3] H. Yoshiara, H. Hasegawa, H. Kanai, and M. Tanaka, "Ultrasonic imaging of propagation of contraction and relaxation in the heart walls at high temporal resolution," *Jpn. J. Appl. Phys.*, vol. 46, no. 7B, pp. 4889–4896, 2007.

[4] H. Kanai, "Propagation of spontaneously actuated pulsive vibration in human heart wall and *in vivo* viscoelasticity estimation," *IEEE Trans. Ultrason. Ferroelectr. Freq. Control*, vol. 52, no. 11, pp. 1931–1942, 2005.

[5] D. M. Bers, *Excitation-Contraction Coupling and Cardiac Contractile Force*, 2nd ed., Dordrecht, The Netherlands: Kluwer Academic, 2001.

[6] E. Konofagou, J. Luo, K. Fujikura, D. Cervantes, and J. Coromilas, "Imaging the electromechanical wave imaging of cardiovascular tissue *in vivo*," in *Proc. IEEE Ultrasonics Symp.*, 2006, pp. 985–988.

[7] E. E. Konofagou, J. D'hooge, and J. Ophir, "Myocardial elastography—A feasibility study *in vivo*," *Ultrasound Med. Biol.*, vol. 28, no. 4, pp. 475–482, 2002.

[8] J. D'hooge, E. Konofagou, F. Jamal, A. Heimdal, L. Barrios, B. Bijnens, J. Thoen, F. van de Werf, G. Sutherland, and P. Suetens, "Two-dimensional ultrasonic strain rate measurement of the human heart *in vivo*," *IEEE Trans. Ultrason. Ferroelectr. Freq. Control*, vol. 49, no. 2, pp. 281–286, 2002.

[9] H. Kanai and Y. Koiwa, "Myocardial rapid velocity distribution," *Ultrasound Med. Biol.*, vol. 27, no. 4, pp. 481–498, 2001.

[10] D. P. Shattuck, M. D. Weinshenker, S. W. Smith, and O. T. v. Ramm, "Explososcan: A parallel processing technique for high speed ultrasound imaging with linear phased arrays," *J. Acoust. Soc. Am.*, vol. 75, no. 4, pp. 1273–1282, 1984.

[11] J. Lu, "2D and 3D high frame rate imaging with limited diffraction beams," *IEEE Trans. Ultrason. Ferroelectr. Freq. Control*, vol. 44, no. 4, pp. 839–856, 1997.

[12] J. Lu, "Experimental study of high frame rate imaging with limited diffraction beams," *IEEE Trans. Ultrason. Ferroelectr. Freq. Control*, vol. 45, no. 1, pp. 84–97, 1998.

[13] J. Cheng and J. Lu, "Extended high-frame rate imaging method with limited-diffraction beams," *IEEE Trans. Ultrason. Ferroelectr. Freq. Control*, vol. 53, no. 5, pp. 880–899, 2006.

[14] J. Lu, J. Cheng, and J. Wang, "High frame rate imaging system for limited diffraction array beam imaging with square-wave aperture weightings," *IEEE Trans. Ultrason. Ferroelectr. Freq. Control*, vol. 53, no. 10, pp. 1796–1812, 2006.

[15] H. Hasegawa and H. Kanai, "High-frame-rate echocardiography using diverging transmit beams and parallel receive beamforming," *J. Med. Ultrasound*, vol. 38, no. 3, pp. 129–140, 2011.

[16] M. O'Donnell and L. J. Thomas, "Efficient synthetic aperture imaging from a circular aperture with possible application to catheter-based imaging," *IEEE Trans. Ultrason. Ferroelectr. Freq. Control*, vol. 39, no. 3, pp. 366–380, 1992.http://www.ncbi.nlm.nih.gov/entrez/query.fcgi?cmd=Retrieve&db=PubMed&list_uids=18267646&dopt=Abstract

[17] M. Karaman and M. O'Donnell, "Synthetic aperture imaging for small scale systems," *IEEE Trans. Ultrason. Ferroelectr. Freq. Control*, vol. 42, no. 3, pp. 429–442, 1995.

[18] F. Gran and J. A. Jensen, "Directional velocity estimation using a spatio-temporal encoding technique based on frequency division for synthetic transmit aperture ultrasound," *IEEE Trans. Ultrason. Ferroelectr. Freq. Control*, vol. 53, no. 7, pp. 1289–1299, 2006.

[19] J. Camacho, M. Parrilla, and C. Fritsch, "Phase coherence imaging," *IEEE Trans. Ultrason. Ferroelectr. Freq. Control*, vol. 56, no. 5, pp. 958–974, 2009.

[20] G. C. Carter, C. H. Knapp, and A. H. Nuttall, "Estimation of the magnitude-squared coherence function via overlapped fast Fourier transform processing," *IEEE Trans. Audio Electroacoust.*, vol. AU-21, no. 4, pp. 337–344, 1983.

Osteoporos Int (2012) 23:1673–1681
DOI 10.1007/s00198-011-1753-4

ORIGINAL ARTICLE

Skin advanced glycation end-product accumulation is negatively associated with calcaneal osteo-sono assessment index among non-diabetic adult Japanese men

H. Momma · K. Niu · Y. Kobayashi · L. Guan · M. Sato · H. Guo · M. Chujo · A. Otomo · C. Yufei · H. Tadaura · T. Saito · T. Mori · T. Miyata · R. Nagatomi

Received: 13 April 2011 / Accepted: 10 August 2011 / Published online: 8 September 2011

Abstract
Summary This study aims to determine the relationship between advanced glycation end-product (AGE) accumulation in skin tissue and bone strength, assessed by quantitative ultrasound, among healthy adult Japanese men. The results of the study suggest that men with higher AGE accumulation in skin tissue have a lower osteo-sono assessment index.
Introduction AGE accumulate in bone collagen with age and diabetes and decrease the mechanical properties of bone. Although increased AGE levels are associated with fractures among diabetic patients and elderly women, it is unclear whether a relationship between increased AGE levels and bone strength is present in apparently healthy adult males. The aim of this study was to determine the relationship between AGE accumulation in tissue and the mechanical properties of bone among adult Japanese men, using quantitative ultrasound as a surrogate measure of the latter.
Methods Skin autofluorescence (AF), which is a noninvasive method for measuring tissue AGEs, and osteo-sono assessment index (OSI), which is determined by quantitative ultrasound, were measured in 193 adult Japanese men (median age 43 years; interquartile range 37.0–55.0 years).
Results Adjusted for age, BMI, calcium intake, physical activity, smoking status, and education level, log-transformed skin AF had a negative association with log-transformed OSI (β=−0.218, P<0.01). Adjusted geometric means (95% CI) for OSI across the tertiles of skin AF were 2.81 (2.75–2.87) for the lowest tertile, 2.81 (2.74–2.87) for the middle tertile, and 2.66 (2.61–2.73) for the highest tertile; thus, OSI for the highest skin AF appeared to be 5.0% lower than that for the lowest and middle skin AF tertiles (P<0.01).
Conclusion Among apparently healthy adult Japanese men, those with higher skin AF had a lower OSI, indicating a relationship between AGE accumulation and bone strength. A long-term prospective study is required to clarify the causality.

Keywords Advanced glycation end-products · Bone quality · Bone strength · Carbonyl stress · Oxidative stress · Quantitative ultrasound

H. Momma · K. Niu · T. Saito · R. Nagatomi (✉)
Division of Biomedical Engineering for Health and Welfare,
Tohoku University Graduate School of Biomedical Engineering,
2-1 Seiryo-machi, Aoba-ku,
Sendai 980-8575, Japan
e-mail: nagatomi@med.tohoku.ac.jp

Y. Kobayashi · L. Guan · M. Sato · H. Guo · M. Chujo · A. Otomo · C. Yufei · H. Tadaura
Department of Medicine and Science in Sports and Exercise,
Tohoku University Graduate School of Medicine,
Sendai, Japan

T. Mori · T. Miyata
United Centers for Advanced Research and Translational Medicine,
Tohoku University Graduate School of Medicine,
Sendai, Japan

Introduction

Osteoporosis is a critical public health problem due to its association with bone fragility and susceptibility to fracture [1]. According to the U.S. National Institutes of Health, osteoporosis is defined as a systemic skeletal disorder characterized by compromised bone strength [2]. Bone strength is not only determined by measures of bone density, such as mass and mineral density, but also by bone quality,

including microarchitecture, turnover, accumulation of microdamage, mineralization, and quality of collagens [2, 3]. Interestingly, patients with type 2 diabetes have an increased risk of fracture despite normal or high bone mineral density (BMD) compared with non-diabetic controls, suggesting poorer bone quality in diabetic patients [4].

Accumulation of advanced glycation end-products (AGEs), which are often found in diabetic patients, in bone collagen has been proposed as a factor responsible for reducing bone strength with aging [5], diabetes [6, 7], and osteoporosis [8–10]. AGEs are a diverse class of compounds resulting from non-enzymatic reactions between glucose and proteins. A common consequence of AGE formation is covalent cross-linking, mostly to proteins including collagen. Accumulation of AGEs in bone collagen decreases the mechanical properties of bone collagen [11, 12]. In rats, an increase of AGE content in bone decreases the mechanical properties of bone despite normal BMD [6]. In humans, the AGE concentration of cortical bone shows a significant increase with age and is negatively correlated with osteoporotic index (Singh score) [5]. Moreover, the AGE content in bone is higher in patients with hip fracture than in subjects without fractures [10].

In a population study, Shiraki et al. demonstrated that a high level of urinary pentosidine, a major AGE in vivo, was an independent risk factor for osteoporotic vertebral fractures in elderly women [13]. Schwartz et al. reported that urinary pentosidine content was associated with increased fracture incidence in older adults with diabetes [14]. The subjects of these studies were older adults who had an increased risk of life-related diseases, such as diabetes and osteoporosis. However, AGEs may accumulate before the onset of diabetes and even at a younger age. In non-diabetic Japanese subjects, serum AGE levels were independently correlated with insulin resistance, which may gradually cause diabetes [15]. Pentosidine content in bone or serum increased with advancing age [5]. Given that bone strength commonly peaks when a person is in his/her 20s and then gradually declines with advancing age, AGE accumulation may be associated with bone strength, if not with fractures, preclinically. Moreover, in men, the lifetime risk of any osteoporotic fracture has been assessed as being within the range 13–22% [1], so osteoporosis is no longer a problem only for women and the elderly. Greater AGE accumulation may potentially be related to poorer bone strength in apparently healthy adult men.

Thus, in this study, we examined the association between skin autofluorescence (AF), which is associated with skin accumulation of AGEs, including pentosidine [16], and quantitative ultrasound examination of calcaneal bone, which correlates with mechanical properties of the bone and may have a predictive value for hip fractures in men [17], among apparently healthy adult men. We hypothesized that skin AF would have a negative association with quantitative ultrasound among adult men.

Methods

Study participants

The study participants consisted of adult male employees enrolled in a prospective study of risk factors for lifestyle-related illnesses or health status in Japan. Participants received annual health examinations including anthropometric measurements, hematological examinations, and, in 2009, an additional assessment including the accumulation of AGEs in skin and quantitative ultrasound examination of calcaneal bone. This study was carried out during the first week (from Monday to Friday) of August. The details of this study have been described elsewhere [18, 19].

The sample selection process is described in Fig. 1. In 2009, 1,263 participants had undergone health examinations for lifestyle-related illnesses. Of these, 1,215 (933 men) participated in our survey and provided their informed consent for data analysis (response rate, 96.2%). Those who underwent skin AF measurement were randomly selected (n=518). Two hundred seventy-two (272) participants who had a low skin reflection (<10%) were excluded (details are provided in the Skin autofluorescence section below). Furthermore, we excluded 52 men who had and/or were receiving treatment for a disease that could influence bone metabolism (osteoporosis, rheumatoid arthritis, hyper- or hypothyroidism, hyper- or hypoparathyroidism, diabetes mellitus, renal dysfunction, or corticosteroid use); one man was excluded because of incomplete data. As a result, 193 men were included in the present study. None had a history of vertebral fractures. The protocol of this study was approved by the Institutional Review Board of the Tohoku University Graduate School of Medicine.

Skin autofluorescence

AGE accumulation in skin tissue was assessed on the basis of skin AF, using an AF reader (AGE Reader; DiagnOptics, Groningen, The Netherlands), as described previously [16]. The AGE Reader consists of a tabletop box equipped with an excitation light source. Each measurement took approximately 30 s to complete and was performed by an independent observer. Excitation light of 300–420-nm wavelength was projected onto the skin surface through a 1-cm^2 hole. The intensity of light emitted from the skin at wavelengths between 420 and 600 nm was measured with a

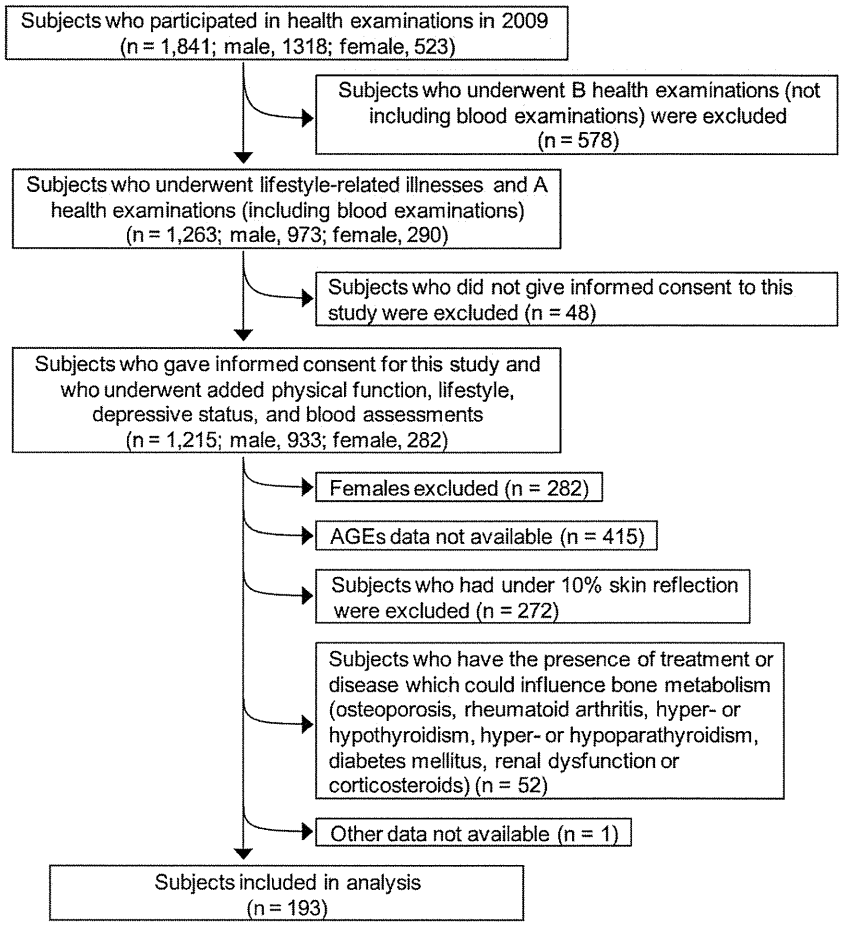

Fig. 1 Flow chart of the sample selection process AGEs, advanced glycation end-products

spectrometer via a glass fiber. Skin AF was calculated by dividing the mean value of the emitted light intensity per nanometer between 420 and 600 nm by the mean value of the excitation light intensity per nm between 300 and 420 nm; the result was expressed in arbitrary unit (AU) and multiplied by 100 for easier evaluation. The intra- and inter-assay coefficients of variation for AGE reader measurement were 2.9–1.8%, respectively.

All AF measurements were performed at room temperature on the volar side of the lower right arm, approximately 10–15 cm below the elbow fold, with the participants in a seated position. Care was taken to perform the measurement at a normal skin site without visible vessels, scars, lichenification, or other skin abnormalities. The arm of each subject was covered with a black cloth to avoid any influence of external light during the measurement. Because creams and sunscreens can affect skin AF measurement [20], we asked each participant whether they applied creams or sunscreens on their arms when skin AF was measured. No participants applied any creams or sunscreens. Since skin pigmentation influences AF measurements, particularly when skin reflection is below 10%, AF values were not used if the skin reflection was below 10% [21].

Quantitative ultrasound assessment of the calcaneus

Quantitative ultrasound assessment of the calcaneus was performed using an ultrasound system (AOS-100; Aloka Co. Ltd., Tokyo, Japan). The AOS-100 measured the speed of sound (SOS) as an index of bone density and the transmission index (TI) as an index of bone structure. The osteo-sono assessment index (OSI) was calculated using the following formula: $OSI=TI\times SOS^2$. OSI provides information on bone stiffness in a radiation-free, convenient, and portable manner. Because this study was conducted along with annual health examinations, a rapid and simple measurement was prerequisite. The intra- and inter-assay coefficients of variation for the OSI were 1.1–0.8%, respectively.

Assessment of other variables

Blood samples were drawn from the antecubital vein, with minimal tourniquet use, while the subjects were seated. Specimens were collected in siliconized vacuum glass tubes containing sodium fluoride for fasting blood glucose and no additives for lipid analyses. Fasting blood glucose concentration was measured by enzymatic methods (Eerotec,

Tokyo, Japan). The triglyceride (TG), low-density lipoprotein cholesterol (LDL-C), and high-density lipoprotein cholesterol (HDL-C) concentrations were measured by enzymatic methods using appropriate kits (Sekisui Medical, Tokyo, Japan).

Depressive symptoms were assessed according to the Japanese version [22] of the Self-Rating Depression Scale (SDS). Participants were considered as depressive when the SDS score was 45 or more [23].

Blood pressure (BP) in the left upper arm was measured twice using an automatic device (YAMASU605P; Kenzmedico Co. Ltd., Saitama, Japan) following a 5-min rest in a seated position. The mean value was used as the BP value.

Anthropometric parameters (height and body weight) were recorded using a standard protocol. Body mass index (BMI) was calculated as weight (kilogram) divided by height in meters squared. Sociodemographic variables, including age and educational level, were also assessed. Educational level was assessed by determining the final grade level and was divided into two categories: lower than college level and college level and above. History of physical illness and current medication use were evaluated on the basis of "yes" or "no" responses to questions. History of fractures was obtained from a questionnaire owing to the unavailability of clinical data and was divided into two categories: those who had a history of lower extremity fractures and those who did not. Information on smoking status (never, former, or currently smoking and Brinkman index), alcohol-drinking status (never, ≥1 day/week, or 7 days/week), and occupation (desk based or not), was obtained from a questionnaire survey. Levels of daily physical activity (PA) were estimated using the International Physical Activity Questionnaire (Japanese version) [24], and categorized into tertiles (low, middle, and high). Calcium, vitamin D, and alcohol intake were estimated using a brief self-administered dietary history questionnaire [25]. A diagnosis of metabolic syndrome (MS) was defined according to the modified Japanese criteria (defined by the Japanese Society for the Study of Obesity) [26].

Statistical analysis

All statistical analyses were performed using SPSS 17.0 for Windows (SPSS, Inc., Chicago, IL, USA).

In this study, because the distribution of all continuous variables except for systolic BP was not normal, the natural logarithm was applied to normalize the data before statistical analysis (analysis of variance [ANOVA], analysis of covariance [ANCOVA], and linear regression analysis). Descriptive statistics were computed for each variable by using logistic regression analysis and ANOVA. Descriptive data are represented as the median (interquartile range) for non-adjusted continuous variables, geometric means (95% confidence interval [CI]) for adjusted continuous variables, and percentages for categorical variables. Linear regression analysis was used to examine the relationship between log-transformed skin AF and other factors with log-transformed OSI. All variables included in Table 1 were analyzed by univariable linear regression. Variables that were at a level of significance of $P<0.10$ in univariate analyses were included in the multivariate models. Multiple linear regression analysis was performed to determine the independent relationship of variables with log-transformed OSI. ANCOVA using log-transformed OSI as the dependent variable and the tertiles of skin AF as independent variables was performed with adjustment for the same variables as in the multiple linear regression models. Bonferroni-corrected P values were used for comparisons between groups differing in skin AF. All tests for statistical significance were two-sided, and $P<0.05$ was defined as statistically significant.

Results

Characteristics of the 193 study participants are shown in Table 1. Overall, median (interquartile range) OSI was 2.75 (2.59–2.93), and skin AF was 1.96 (1.78–2.14) AU. Median age was 45.0 years.

In the univariate analyses (Table 2), log-transformed OSI was significantly associated with age, BMI, calcium intake, high PA, former smoker, and skin AF. The association of log-transformed OSI with waist circumference, education level (college level and above), and MS were borderline significance, and there was no association of log-transformed OSI with fasting blood glucose, TG, LDL-C, HDL-C, BP, vitamin D intake, middle PA, current smoker, drinking status, depressive symptoms (SDS≥45), desk work, and leg fracture. Among current smokers, Brinkman index was associated with OSI ($r=-0.16$, $P=0.04$, data not shown).

To determine whether skin AF was independently associated with OSI, we performed a multiple linear regression analysis using skin AF and other variables associated with OSI in the univariate analyses (Table 3). Although waist circumference had a tendency to associate with OSI in the univariate model, waist circumference was not included in the multivariate model since it was strongly correlated with BMI. After adjustment for age, BMI, calcium intake, PA level, smoking status, education level, and MS, log-transformed skin AF had a negative association with log-transformed OSI ($\beta=-0.218$, SE=0.069, $P<0.01$). Table 4 shows the relationship of the tertiles of skin AF with log-transformed OSI using ANCOVA. The adjusted geometric mean (95% CI) of log-transformed OSI across the tertiles of skin AF was 2.81 (2.75–2.87) for the lowest tertile, 2.81 (2.74–2.87) for the middle tertile,

Table 1 Characteristics of participants (n=193)

Characteristic	Median (interquartile range) or percentage, %
Age (years)	45.0 (37.0–55.0)
BMI (kg/m^2)	23.7 (21.9–25.8)
Waist circumference (cm)	85.0 (79.0–91.0)
SBP (mm Hg)	128.0 (118.0–138.0)
DBP (mm Hg)	80.0 (74.0–90.0)
Fasting blood glucose (mg/dL)	93.0 (88.0–100.0)
TG (mg/dL)	128.0 (77.0–183.0)
LDL-C (mg/dL)	121.0 (103.0–140.0)
HDL-C (mg/dL)	52.0 (43.0–58.0)
Calcium intake (mg/day·2,000 kcal)	460.1 (349.1–606.8)
Vitamin D intake (mg/day·2,000 kcal)	10.8 (7.1–16.0)
High PA (median values, 48.0 METs h/week)	33.2
Middle PA (median values, 12.0 METs h/week)	33.2
Smoking status	
Current	40.3
Former	13.7
Drinking status	
7 drinks/week	28.0
≥1 drink(s)/week	55.9
Depressive symptoms (SDS≥45)	29.9
Education (≥college)	38.4
Desk work	79.6
Leg fracture	16.6
MS (JASSO)	22.7
Skin AF	1.96 (1.78–2.14)
OSI	2.75 (2.59–2.93)

BMI body mass index, *SBP* systolic blood pressure, *DBP* diastolic blood pressure, *TG* triglyceride, *LDL-C* low-density lipoprotein cholesterol, *HDL-C* high-density lipoprotein cholesterol, *PA* physical activity, *SDS* Self-rating Depression Scale, *MS* metabolic syndrome, *JASSO* Japanese Society for the Study of Obesity, *AF* autofluorescence, *OSI* osteo-sono assessment index

and 2.66 (2.61–2.73) for the highest tertile; thus, participants in the highest tertile had 5.0% lower OSI than those in the lowest and middle tertiles (Bonferroni-corrected P value<0.01).

Discussion

The present study examined the relationship between skin AF associated with AGE accumulation and OSI, a quantitative ultrasound measure, among non-diabetic adult Japanese men. Consistent with our hypothesis, our results showed that levels of skin AF were independently associated with OSI, suggesting that participants with higher skin AF had lower OSI.

In previous population studies, the relationship between AGE accumulation and fracture risk has been controversial. Some studies reported that there was no association between urinary pentosidine and fracture risk after adjustment in non-diabetic older Caucasian [14] and among postmenopausal Caucasian women [27]. On the other hand, in elderly Japanese women, a high level of urinary pentosidine was an independent risk factor for osteoporotic vertebral fractures [13]. Possibly in line with these findings, we found a negative association between skin AF with OSI among adult Japanese men after adjustment for potential confounders, given that lower OSI may lead to higher fracture risk. Although the reasons for this discrepancy are unknown, racial differences may potentially explain the inconsistent results of the studies. While Japanese have twice the incidence of the methylenetetrahydrofolate reductase polymorphism (C677T) compared with Caucasians, Japanese subjects are predisposed to mild hyperhomocysteinemia [28–30]. Indeed, hyperhomocysteinemia caused a reduction in bone toughness through the accumulation of pentosidine in bone in rabbit models [31]. Other explanation could be diet, which is a major source of exogenous AGEs [32]. AGEs are especially high in Western diet, since heat-treated process enhances the formation of AGEs [32], and the concentration of urinary pentosidine in Caucasian women [27] was more than twofold greater than that in Japanese women [13]. Therefore, Japanese who may be ingesting less dietary AGE might be more susceptible to the adverse effect of AGE accumulation.

Table 2 Univariate linear regression models of skin AF and other factors with OSI

Characteristic	β	*P* value
Age (years)	−0.26	<0.01
BMI (kg/m^2)	0.20	<0.01
Waist circumference (cm)	0.13	0.06
SBP (mm Hg)	0.03	0.67
DBP (mm Hg)	0.01	0.91
Fasting blood glucose (mg/dL)	−0.10	0.16
TG (mg/dL)	−0.10	0.92
LDL-C (mg/dL)	0.03	0.72
HDL-C (mg/dL)	−0.01	0.85
Calcium intake (mg/day·2,000 kcal)	0.15	0.03
Vitamin D intake (mg/day·2,000 kcal)	0.03	0.64
High PA (median values, 48.0 METs h/week)[a]	0.15	0.03
Middle PA (median values, 12.0 METs h/week)[a]	−0.07	0.30
Smoking status[b]		
Current	−0.03	0.69
Former	−0.15	0.03
Drinking status[c]		
7 drinks/week	−0.06	0.42
≥1 drinks/week	0.09	0.18
Depressive symptoms (SDS≥45)	−0.05	0.49
Education (≥college)	0.12	0.07
Desk work	0.06	0.42
Leg fracture	0.08	0.22
MS (JASSO)	0.13	0.05
Skin AF	−0.25	<0.01

OSI osteo-sono assessment index, *BMI* body mass index, *SBP* systolic blood pressure, *DBP* diastolic blood pressure, *TG* triglyceride, *LDL-C* low-density lipoprotein cholesterol, *HDL-C* high-density lipoprotein cholesterol, *PA* physical activity, *SDS* Self-rating Depression Scale, *MS* metabolic syndrome, *JASSO* Japanese Society for the Study of Obesity, *AF* autofluorescence

[a]Reference category is low PA

[b]Reference category is never

[c]Reference category is ≤1 drink/week

Skin AF measurement is a noninvasive, rapid, and highly reproducible method, which effectively measures tissue AGE accumulation. This method has been validated to correspond to specific AGE skin levels, including pentosidine [16]. As for the clinical significance of skin AF measurement, however, we still have a limited number of prospective studies in which Skin AF was shown to predict developments of diabetic complications [33], and was associated with all-cause mortality [34] in type 2 diabetes in a prospective study with a follow-up period of 3.1 years. Therefore, more prospective studies with larger sample size and longer follow-up period are necessary to establish its clinical significance.

Table 3 Multiple linear regression models of log-transformed skin AF with log-transformed OSI

Characteristic	β	SE	*P* value
Participants (n=193)			
Log-skin AF	−0.218	0.069	<0.01

Adjusted for age, body mass index, calcium intake, physical activity level, smoking status, education level, and metabolic syndrome

AF autofluorescence, *OSI* osteo-sono assessment index, *SE* standard error

Table 4 Relationship of the tertile of skin autofluorescence (AF) with log-transformed OSI among adult Japanese men

	Tertiles of skin AF		
Range (unit, AU)	Low (1.28–1.82)	Middle (1.82–2.05)	High (2.05–2.88)
Number of participants	65	64	64
Crude	2.83 (2.76–2.90)	2.78 (2.71–2.85)	2.68 (2.61–2.74)*
Adjusted[a]	2.81 (2.75–2.87)	2.81 (2.74–2.87)	2.66(2.61–2.73)*,**

Data are geometric means (95% confidence interval). Unit of leg extension power is watts per kilogram

Analysis of variance or analysis of covariance

* P<0.01; significantly different from lowest skin autofluorescence tertile (Bonferroni correction)

** P<0.01; significantly different from middle skin autofluorescence tertile (Bonferroni correction)

[a] Adjusted for age, body mass index, calcium intake, physical activity level, smoking status, education level, and metabolic syndrome

Sell et al. have shown an exponential increase in pentosidine accumulation across the age in skin collagen [35]. In a separate study, Odetti et al. have shown a similar exponential increase in pentosidine accumulation across the age in bone collagen [5]. Interestingly, the level of pentosidine per unit collagen is higher in the bone as compared to the skin. This difference well corresponds to the result obtained in a cadaver study in which post-mortem bodies of human were analyzed [36]. They showed that pentosidine level per milligram of collagen was more than 60% higher in the bone tissue as compared to the skin tissue. Taken together, skin and bone pentosidine levels are likely to have a positive correlation. Further study is necessary to establish this relationship, but we believe that skin AF may not only correspond to skin pentosidine accumulation, but also bone pentosidine accumulation. In rats, the accumulation of pentosidine in bone was significantly associated with the reduction of bone stiffness [7]. Although the cause–effect relationship cannot be established in this cross-sectional design, we believe that skin AF may be associated with bone strength. Further prospective study is, therefore, required to establish the prospective value of skin AF on bone strength.

In the present study, we used OSI as an index of bone strength. Although OSI is not widely used to assess bone strength, quantitative ultrasound (QUS) parameters including OSI may reflect not only bone mass but also bone quality. A previous study found that impaired bone mechanical properties in diabetic rats coincided with impaired enzymatic cross-link formation and increases in glycation-induced pentosidine, despite the lack of reduction in BMD [7], therefore, it is possible that AGE accumulation may more clearly be associated with OSI rather than BMD which measures bone density. In this study, OSI was 5.0% lower for the highest skin AF compared with the lowest and middle skin AFs after adjustment for confounders. Njeh et al. showed that patients with hip fractures had 8.0% lower OSI compared with control subjects [37]. Therefore, the influence of preclinical AGE accumulation in bone tissue may not be negligible.

Our finding is consistent with the observation in in vitro studies that increased AGE level in bone collagen reduces bone mechanical properties [11, 12]. AGE accumulation significantly alters the quantity and morphology of microdamage and results in reduced fracture resistance [38]. Moreover, in spontaneously diabetic rats, decreased mechanical properties of femoral bone are accompanied by increased accumulation of pentosidine, and the pentosidine content is significantly associated with the mechanical properties of bone [6]. Indeed, in several studies, patients with hip fractures had higher bone pentosidine content [9, 10] or serum AGEs [8] compared with subjects without fractures.

In addition to the adverse effects of AGEs on the material properties of bone collagen, AGE accumulation may potentially influence bone cells. AGE-modified bone collagen has detrimental effects on osteoblastic function [7, 39]. The effects of AGEs on osteoclastic bone resorption are controversial. Receptor-of-AGE (RAGE) knockout mice have significantly higher bone mechanical strength, probably due to decreased number of osteoclasts compared with wild-type mice [40]. Furthermore, Miyata et al. showed that AGEs increased the number of resorption pits in cultured mouse bone cells as well as when AGE-accumulated bone particles were implanted subcutaneously in rats [41]. In contrast, Valcourt et al. reported that bone resorption was inhibited in an in vitro study using rabbit and human mature osteoclasts seeded on AGE-modified slices [42]. AGEs also inhibited the proliferation of human mesenchymal stem cells and cognate differentiation into bone [43].

Although there was no association between smoking status and OSI in this study, Brinkman index was negatively associated with OSI among current smokers. Therefore, smoking may have harmful effect on bone strength among healthy adult men. As for drinking status, we found no association with OSI. A previous study reported that, among Korean men, four to seven cups of soju (the most popular liquor in Korea) is associated with the risk of reduced QUS parameters [44]. When the amount of alcohol intake in our population was converted to alcohol amount per a cup of soju, only less than 20% of our participants drank the amount of alcohol corresponded to four or more cups of soju (data not shown). Thus, it is possible that the alcohol intake in our study was small in the previous study [44].

This study has some limitations. First, although we adjusted for confounders such as lifestyle factors and disease, we could not exclude the possibility that bone strength was affected by other factors associated with lifestyle or disease. Moreover, because this study was a cross-sectional study, we could not conclude whether AGE accumulation in skin tissue reduced bone strength. A larger population-based prospective study should be performed to further confirm the causal relationship between skin AGE accumulation and bone strength.

In conclusion, in apparently healthy adult Japanese men, skin AF was independently associated with OSI, suggesting that the participants with higher skin AF had a lower OSI. Further studies are needed to confirm the causal relationship between skin AGE accumulation and bone strength.

Acknowledgments We gratefully acknowledge all the subjects participating in our study and the Sendai Oroshisho Center for allowing us to perform the study. This work was supported by "Knowledge Cluster Initiative" from the Ministry of Education, Culture, Sports, Science and Technology of Japan.

Conflicts of interest None.

References

1. Johnell O, Kanis J (2005) Epidemiology of osteoporotic fractures. Osteoporos Int 16(Suppl 2):S3–S7
2. Anonymous (2001) Osteoporosis prevention, diagnosis, and therapy. JAMA 285:785–795
3. Viguet-Carrin S, Garnero P, Delmas PD (2006) The role of collagen in bone strength. Osteoporos Int 17:319–336
4. Schwartz AV, Sellmeyer DE, Ensrud KE, Cauley JA, Tabor HK, Schreiner PJ, Jamal SA, Black DM, Cummings SR (2001) Older women with diabetes have an increased risk of fracture: a prospective study. J Clin Endocrinol Metab 86:32–38
5. Odetti P, Rossi S, Monacelli F, Poggi A, Cirnigliaro M, Federici M, Federici A (2005) Advanced glycation end products and bone loss during aging. Ann N Y Acad Sci 1043:710–717
6. Katayama Y, Akatsu T, Yamamoto M, Kugai N, Nagata N (1996) Role of nonenzymatic glycosylation of type I collagen in diabetic osteopenia. J Bone Miner Res 11:931–937
7. Saito M, Fujii K, Mori Y, Marumo K (2006) Role of collagen enzymatic and glycation induced cross-links as a determinant of bone quality in spontaneously diabetic WBN/Kob rats. Osteoporos Int 17:1514–1523
8. Hein G, Wiegand R, Lehmann G, Stein G, Franke S (2003) Advanced glycation end-products pentosidine and N epsilon-carboxymethyllysine are elevated in serum of patients with osteoporosis. Rheumatology 42:1242–1246
9. Saito M, Fujii K, Marumo K (2006) Degree of mineralization-related collagen crosslinking in the femoral neck cancellous bone in cases of hip fracture and controls. Calcif Tissue Int 79:160–168
10. Saito M, Fujii K, Soshi S, Tanaka T (2006) Reductions in degree of mineralization and enzymatic collagen cross-links and increases in glycation-induced pentosidine in the femoral neck cortex in cases of femoral neck fracture. Osteoporos Int 17:986–995
11. Garnero P, Borel O, Gineyts E, Duboeuf F, Solberg H, Bouxsein ML, Christiansen C, Delmas PD (2006) Extracellular post-translational modifications of collagen are major determinants of biomechanical properties of fetal bovine cortical bone. Bone 38:300–309
12. Viguet-Carrin S, Farlay D, Bala Y, Munoz F, Bouxsein ML, Delmas PD (2008) An in vitro model to test the contribution of advanced glycation end products to bone biomechanical properties. Bone 42:139–149
13. Shiraki M, Kuroda T, Tanaka S, Saito M, Fukunaga M, Nakamura T (2008) Nonenzymatic collagen cross-links induced by glycoxidation (pentosidine) predicts vertebral fractures. J Bone Miner Metab 26:93–100
14. Schwartz AV, Garnero P, Hillier TA, Sellmeyer DE, Strotmeyer ES, Feingold KR, Resnick HE, Tylavsky FA, Black DM, Cummings SR, Harris TB, Bauer DC (2009) Pentosidine and increased fracture risk in older adults with type 2 diabetes. J Clin Endocrinol Metab 94:2380–2386
15. Tahara N, Yamagishi SI, Matsui T, Takeuchi M, Nitta Y, Kodama N, Mizoguchi M, Imaizumi T (2010) Serum levels of advanced glycation end products (AGEs) are independent correlates of insulin resistance in nondiabetic subjects. Cardiovasc Ther. doi:10.1111/j.1755-5922.2010.00177.x
16. Meerwaldt R, Graaff R, Oomen PH, Links TP, Jager JJ, Alderson NL, Thorpe SR, Baynes JW, Gans RO, Smit AJ (2004) Simple non-invasive assessment of advanced glycation endproduct accumulation. Diabetologia 47:1324–1330
17. Fujiwara S, Sone T, Yamazaki K, Yoshimura N, Nakatsuka K, Masunari N, Fujita S, Kushida K, Fukunaga M (2005) Heel bone ultrasound predicts non-spine fracture in Japanese men and women. Osteoporos Int 16:2107–2112
18. Guo H, Niu K, Monma H, Kobayashi Y, Guan L, Sato M, Minamishima D, Nagatomi R (2010) Association of Japanese dietary pattern with serum adiponectin concentration in Japanese adult men. Nutr Metab Cardiovasc Dis. doi:101016/jnumecd201006006
19. Momma H, Niu K, Kobayashi Y, Guan L, Sato M, Guo H, Chujo M, Otomo A, Yufei C, Tadaura H, Saito T, Mori T, Miyata T, Nagatomi R (2010) Skin advanced glycation end product accumulation and muscle strength among adult men. Eur J Appl Physiol 111(7):1545–1552
20. Noordzij MJ, Lefrandt JD, Graaff R, Smit AJ (2011) Dermal factors influencing measurement of skin autofluorescence. Diabetes Technol Ther 13:165–170
21. Na R, Stender IM, Henriksen M, Wulf HC (2001) Autofluorescence of human skin is age-related after correction for skin pigmentation and redness. J Invest Dermatol 116:536–540
22. Fukuda K, Kobayashi S (1973) A study on a self-rating depression scale (author's transl). Seishin Shinkeigaku Zasshi 75:673–679 (in Japanese)
23. Fountoulakis KN, Lacovides A, Samolis S, Kleanthous S, Kaprinis SG, St Kaprinis G, Bech P (2001) Reliability, validity and psychometric properties of the Greek translation of the Zung Depression Rating Scale. BMC Psychiatry 1:6
24. Craig CL, Marshall AL, Sjostrom M, Bauman AE, Booth ML, Ainsworth BE, Pratt M, Ekelund U, Yngve A, Sallis JF, Oja P (2003) International physical activity questionnaire: 12-country reliability and validity. Med Sci Sports Exerc 35:1381–1395
25. Sasaki S (2005) Serum biomarker-based validation of a brief-type self-administered diet history questionnaire for Japanese subjects. A research for assessment of nutrition and dietary habit in "Kenko Nippon 21". The Study Group of Ministry of Health, Labor and Welfare of Japan, Tokyo, Japan, pp 10–42 (in Japanese)
26. Matsuzawa Y (2005) Metabolic syndrome—definition and diagnostic criteria in Japan. J Atheroscler Thromb 12:301
27. Gineyts E, Munoz F, Bertholon C, Sornay-Rendu E, Chapurlat R (2010) Urinary levels of pentosidine and the risk of fracture in postmenopausal women: the OFELY study. Osteoporos Int 21:243–250
28. Loscalzo J (1996) The oxidant stress of hyperhomocyst(e)inemia. J Clin Invest 98:5–7
29. Shiraki M, Urano T, Kuroda T, Saito M, Tanaka S, Miyao-Koshizuka M, Inoue S (2008) The synergistic effect of bone mineral density and methylenetetrahydrofolate reductase (MTHFR) polymorphism (C677T) on fractures. J Bone Miner Metab 26:595–602
30. Saito M, Marumo K (2010) Collagen cross-links as a determinant of bone quality: a possible explanation for bone fragility in aging, osteoporosis, and diabetes mellitus. Osteoporos Int 21:195–214
31. Saito M, Marumo K, Soshi S, Kida Y, Ushiku C, Shinohara A (2010) Raloxifene ameliorates detrimental enzymatic and nonenzymatic collagen cross-links and bone strength in rabbits with hyperhomocysteinemia. Osteoporos Int 21:655–666
32. Goldberg T, Cai W, Peppa M, Dardaine V, Baliga BS, Uribarri J, Vlassara H (2004) Advanced glycoxidation end products in commonly consumed foods. J Am Diet Assoc 104:1287–1291
33. Gerrits EG, Lutgers HL, Kleefstra N, Graaff R, Groenier KH, Smit AJ, Gans RO, Bilo HJ (2008) Skin autofluorescence: a tool

to identify type 2 diabetic patients at risk for developing microvascular complications. Diabetes Care 31:517–521
34. Lutgers HL, Gerrits EG, Graaff R, Links TP, Sluiter WJ, Gans RO, Bilo HJ, Smit AJ (2009) Skin autofluorescence provides additional information to the UK Prospective Diabetes Study (UKPDS) risk score for the estimation of cardiovascular prognosis in type 2 diabetes mellitus. Diabetologia 52:789–797
35. Sell DR, Monnier VM (1990) End-stage renal disease and diabetes catalyze the formation of a pentose-derived crosslink from aging human collagen. J Clin Invest 85:380–384
36. Sell DR, Monnier VM (1989) Structure elucidation of a senescence cross-link from human extracellular matrix. Implication of pentoses in the aging process. J Biol Chem 264:21597–21602
37. Njeh CF, Hans D, Li J, Fan B, Fuerst T, He YQ, Tsuda-Futami E, Lu Y, Wu CY, Genant HK (2000) Comparison of six calcaneal quantitative ultrasound devices: precision and hip fracture discrimination. Osteoporos Int 11:1051–1062
38. Tang SY, Vashishth D (2010) Non-enzymatic glycation alters microdamage formation in human cancellous bone. Bone 46:148–154
39. Sanguineti R, Storace D, Monacelli F, Federici A, Odetti P (2008) Pentosidine effects on human osteoblasts in vitro. Ann N Y Acad Sci 1126:166–172
40. Ding KH, Wang ZZ, Hamrick MW, Deng ZB, Zhou L, Kang B, Yan SL, She JX, Stern DM, Isales CM, Mi QS (2006) Disordered osteoclast formation in RAGE-deficient mouse establishes an essential role for RAGE in diabetes related bone loss. Biochem Biophys Res Commun 340:1091–1097
41. Miyata T, Notoya K, Yoshida K, Horie K, Maeda K, Kurokawa K, Taketomi S (1997) Advanced glycation end products enhance osteoclast-induced bone resorption in cultured mouse unfractionated bone cells and in rats implanted subcutaneously with devitalized bone particles. J Am Soc Nephrol 8:260–270
42. Valcourt U, Merle B, Gineyts E, Viguet-Carrin S, Delmas PD, Garnero P (2007) Non-enzymatic glycation of bone collagen modifies osteoclastic activity and differentiation. J Biol Chem 282:5691–5703
43. Kume S, Kato S, Yamagishi S, Inagaki Y, Ueda S, Arima N, Okawa T, Kojiro M, Nagata K (2005) Advanced glycation end-products attenuate human mesenchymal stem cells and prevent cognate differentiation into adipose tissue, cartilage, and bone. J Bone Miner Res 20:1647–1658
44. Jin LH, Chang SJ, Koh SB, Kim KS, Lee TY, Ryu SY, Song JS, Park JK (2011) Association between alcohol consumption and bone strength in Korean adults: the Korean Genomic Rural Cohort Study. Metabolism 60:351–358

Artificial Organs

Communication

Medical Responses Following the Sendai Quake (East Japan Earthquake, March 11, 2011)

*Tomoyuki Yambe, †Muneichi Shibata, †Taketada Sumiyoshi, †Yoshiaki Mibiki, †Noboru Osawa, ‡Yoshiaki Katahira, ‡Minoru Yambe, ‡Kou-ichi Tabayashi, §Masanori Yamashina, §Eiji Sato, §Shinichi Sato, §Tetsuo Yagi, ¶Makoto Watanabe, ¶Yoshihira Akinno, **Masanori Munakata, ††Naoki Owada, *Masatoshi Akiyama, *Yoshikatsu Saiki, *Norihiro Sugita, and *Makoto Yoshizawa

*Tohoku University, Sendai; †Miyagi Cardiovascular Respiratory Center, Miyagi; ‡Tohoku Kouseinenkin Hospital, Sendai; §Sendai City Hospital, Sendai; ¶Miyagi Shakaihoken Hospital, Sendai; **Tohoku Rosai Hospital, Sendai; and ††Miyagi Cancer Center, Natori, Japan

On March 11, 2011, disaster struck the east coast of Japan (1–7) named of the Great East Japan Earthquake or Sendai Quake (8) (Wikipedia).

Japan had been expecting a large earthquake for a long time. The Sendai Quake involved three epicenters at various distances out to sea. The force of the magnitude 9.0 quake caused an enormous tsunami that deluged the cities on the eastern seashore in the Tohoku area (northeast coast of Japan). In Minamisanriku City, for example, almost all buildings were lost after the earthquake and tsunami struck (Fig. 1).

To add to the disaster, fires broke out after the earthquake and tsunami. Large portions of the cities near the eastern seashore were completely lost. In addition to these disasters, a meltdown occurred at the Fukushima nuclear power plant. Radioactive contamination occurred not only throughout Japan but also all over the world.

Unfortunately, detailed medical data about the aftermath of the Sendai Quake are not available because all medical records were lost with the hospital buildings, especially in the tsunami areas near the eastern seashore. Detailed information of the number of dead has not yet been summarized, even by the Japanese government. As many as 20 000 people have been reported lost as a result of this complex emergency. The medical response following the earthquake and tsunami in eastern Japan has not been clearly described. This short report is intended to provide details of this response.

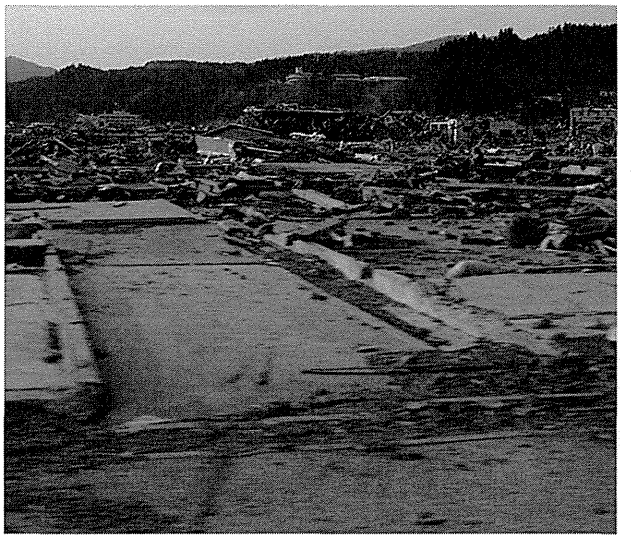

FIG. 1. Minamisanriku City after the tsunami (photo by the Miyagi Medical Support team).

doi:10.1111/j.1525-1594.2012.01522.x

Received January 2012; revised May 2012.

Address correspondence and reprint requests to Dr. Tomoyuki Yambe, Department of Medical Engineering and Cardiology, Tohoku University, 4-1 Seiryo-machi, Aoba-ku, Sendai 980-8575, Japan. E-mail: yambe@idac.tohoku.ac.jp

Presented in part at the 19th Congress of the International Society for Rotary Blood Pumps, held on September 8–10, 2011, in Louisville, KY, USA.

MEDICAL RESPONSE TO THE SENDAI QUAKE

The Tohoku University Hospital is located in Sendai City in the area that sustained the most damage from the tsunami and earthquake. Despite the sadness that flooded the nation after the disaster, one consolation was that no fatalities occurred among patients, doctors, nurses, or other staff at the University Hospital. The response to the disaster at this hospital can be examined in four stages.

The first stage involved initial recovery and preparation for dealing with the aftereffects of the disaster. First, the safety of all patients and staff members was secured. Then, medical resources were mobilized according to the hospital's triage tag system. Everything in the University Hospital was rearranged to accommodate disaster victims. All routine surgeries and medical examinations were postponed, and the outpatient clinic was closed. When disaster victims arrived at the University Hospital, they received green, yellow, red, or black tags, according to the methodology of the triage tag system. Patients with green tags were treated in the outpatient clinic, those with yellow tags went to the intensive care unit, those with red tags went to the operating room, and those with black tags went to the building of basic science. Appropriate treatment was delivered in these various locations.

In the second stage, normal hospital functions were restored. Planning began for the acceptance of patients being transferred from damaged hospitals on the eastern coast. Shortages of all medical resources had been anticipated, so messages were sent to all university hospitals in Japan to gather drugs and food and to prepare disaster medical assistance teams.

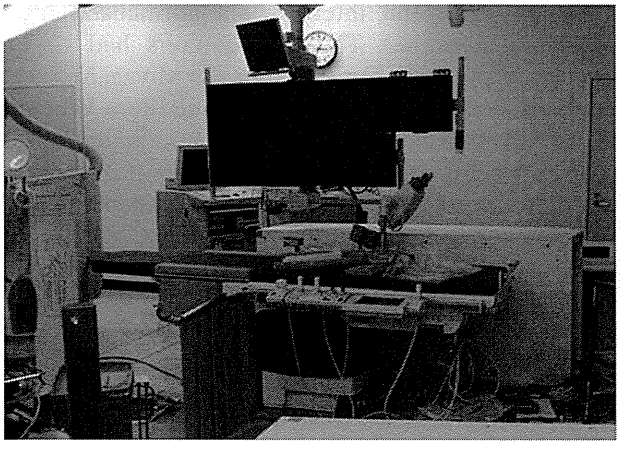

FIG. 2. Cardiac catheterization room after the Sendai Quake.

FIG. 3. Shelter after the tsunami (photo by Miyagi Medical Support Team).

In the third stage, teams of doctors and nurses, along with medical resources, food, and drugs, were sent to the afflicted hospitals. Thousands of medical support teams were sent to the cities on the eastern coast affected by the tsunami. The fourth stage, which involves reconstruction of medical support buildings in the damaged area, is still ongoing.

THE STATE OF MEDICAL CARE AFTER THE TSUNAMI

Challenges were many throughout the region. Creative solutions to various problems had to be sought. For example, in the Miyagi Cardiovascular Respiratory Center, electric power and water supplies were down. Patients in stable condition were therefore discharged, and emergency patients were treated using equipment powered by in-house power generation units.

Despite all the efforts to meet people's needs, medical resources were inadequate because of the magnitude of the disaster. Medical equipment was damaged and debris was everywhere (Fig. 2). Medical teams visited shelters after the tsunami (Fig. 3). The Miyagi Medical Support team diagnosed and treated in a temporary shelter.

An emergency care unit is present at Sendai City Hospital. Although ambulances had been salvaged from the disaster area, destroyed roads and traffic jams prevented them from transporting patients to the hospital. Many patients came to Tohoku Rosai Hospital, located in the city center, on foot. The

volume of patients was large, and the hospital was so busy that medical staff were unable to return to their homes.

Miyagi Shakaihoken Hospital is located near the coast. Many tsunami victims went to that hospital, but the surgery department's systems were down. Patients could not be adequately treated without functional operating rooms.

Some of the most severe damage was observed at Kesennuma City near the seashore. All buildings in that area were destroyed by the earthquake, tsunami, and fire; therefore, people were required to go to refuge centers. Control of hypertension, diabetes, and many other health disorders was difficult in these makeshift conditions, and newly developed electronic doctor's bags were used to control these conditions.

Furthermore, the Sendai Airport was also completely destroyed by the tsunami, but it was restored soon after by the TOMODACHI operation carried out by the US Army.

FUKUSHIMA NUCLEAR POWER PLANT MELTDOWN

The Fukushima nuclear power plant accident exacerbated the already difficult situation in hospitals. On March 11, a meltdown at the power plant was reported, and hydrogen explosions followed on March 12 and 14. Radioactive materials were scattered as a result of these accidents. The plant was shut down.

In Japan, discussion is ongoing concerning the future consequences of the radiation leaks resulting from the accident at Fukushima (9–12). In the early 1960s, Japan experienced a large amount of strontium, cesium, and plutonium fallout caused by atomic bomb experiments conducted by several countries, including the USA, France, the Soviet Union, and China. Plutonium levels in Japan were estimated to be 100 000 times higher in the 1960s compared with recent levels. But the life span of Japanese people is the longest in advanced countries. No one can show the risk of radiation fallout in early 1960s. No increase in cancer incidence was observed in Japan in the early 1960s. Thus, the true risk of radiation fallout is also unclear, because double-blind tests of radiation poisoning cannot be performed.

Sendai City is located north of Fukushima. All roads from Tokyo (south of Fukushima) and other areas of Japan had been blocked between Fukushima and Tokyo, because antinuclear power activists announced a non-scientific propaganda concerning the risk of radiation material fallout. Relief supplies could not be transported into the Fukushima area because of demonstrations by the antinuclear activists. So, the relief goods could not go north to Sendai. Many patients did not survive due to a shortage of drugs and food caused by the propaganda of the antinuclear activists.

USE OF ARTIFICIAL ORGANS DURING THE DISASTER

At the time of the disaster, more than 50 patients were on respirators, whereas 11 were dependent on hemodialysis (HD) at Tohoku University Hospital. Emergency power units ensured the safety of these patients. However, all coastal hospitals had sustained devastating damage. Therefore, all patients who were dependent on HD were transported to Tohoku University Hospital. Medical resources were inadequate to meet their needs, and helicopters transferred these HD patients to other hospitals. Around 100 HD patients were transferred to the other hospitals. In particular, large numbers of HD patients were transferred to Hokkaido.

Three patients required the Nipro ventricular assistance system (VAS) support at Tohoku University Hospital during the Sendai Quake. Because emergency power started smoothly, no disruption of VAS treatment occurred.

However, certain lifelines, such as electric power, water, and gas supplies, had all been shut down in Sendai City. Therefore, patients requiring rotary blood pumps were transported to the ambulance center and subsequently moved to the University Hospital after the roads became passable. Pneumatic VAS remained useful during the disaster, which was surprising because they were situated in the hospital with the emergency power unit.

Patient care had to be performed, although medical resources were limited. For VAS and HD, the prothrombin time and international normalized ratio must be measured. These parameters had to be checked in shelters. For example, the Miyagi Medical Support Team, who visited various shelters, brought electronic medical equipment. This equipment was a lifeline for patients taking refuge in shelters, especially for those requiring life support using artificial organs.

TELEMEDICINE USING THE ELECTRONIC DOCTOR'S BAG

Medical resources were inadequate to respond to the disaster. Medical treatment was limited because all lifelines had been compromised. Doctors and nurses took it upon themselves to visit people in shelters, travelling destroyed roads on foot to do so.

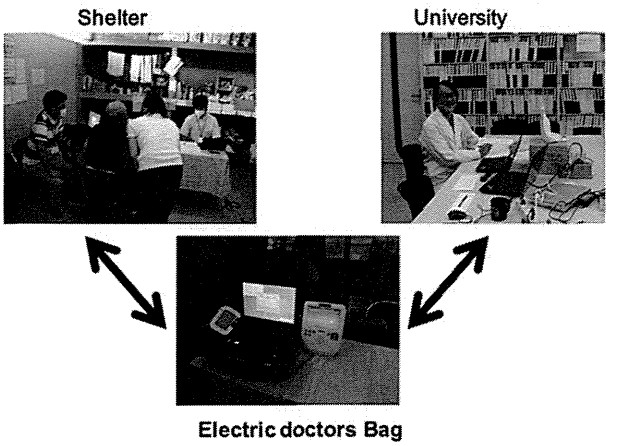

FIG. 4. Above: Clinical application of the electronic doctor's bag in a shelter in Kesennuma City. Below: The bag being tested at Tohoku University.

The electronic doctor's bag, which was invented at Tohoku University, was useful in responding to victims' needs in these emergency conditions (Fig. 4).

The electronic doctor's bag was first used in the shelter in Kesennuma City, one of the most severely damaged areas, after approval from the ethics committee of Tohoku University Graduate School of Medicine. Use of the electronic doctor's bag facilitated evaluation of the condition of patients at the shelter by doctors located at the University. At the time of the disaster, the personnel shortage precluded on-site evaluation. Therefore, telemedicine and remote medicine were thought to be useful. The electronic doctor's bag enabled electrocardiography, blood pressure measurement, and ultrasonic diagnosis to be performed at the disaster shelters. Using this newly developed system, medical personnel in the shelters were also able to confer with doctors at Tohoku University via Skype. Using this device, control of anticoagulation, blood sugar levels, and blood pressure are able to be achieved, thereby preventing adverse cardiovascular events from occurring.

SUMMARY

After the Sendai Quake, all medical resources were mobilized to respond to the disaster. However, shortages of everything caused seemingly insurmountable problems, especially in areas affected by the tsunami. Maintenance of lifelines was vital to patients requiring artificial organs.

Medical equipment preparation and planning are now under way to enable adequate response to future large disasters. Discussion is ongoing about the continued risk of radiation after the Fukushima nuclear power plant meltdown. In previous reports, no risk of increased cancer due to exposure to radiation <100 mSv was reported. In Japan, all radioactive fallout in every area has been reported daily on the governmental website since the disaster. Information about radiation levels is publicly available in Japan.

In conclusion, a detailed statistical analysis of the disaster is now under way, the results of which will be reported in the near future. The most important thing during times of disaster is the rapid recovery of lifelines.

Acknowledgments: The authors express their thanks to the disaster medical assistance teams from all over Japan and the world that provided aid to people in the Tohoku area, and to all hospitals that received and treated the hemodialysis patients. Thanks also to those who participated in the TOMODACHI operation initiated by the US Army for their efforts in restoring the Sendai Airport to operative status and aiding the people of Japan in recovering from the events of March 2011.

REFERENCES

1. Satomi S. The Great East Japan Earthquake: Tohoku University Hospital's efforts and lessons learned. *Surg Today* 2011;41:1171–81.
2. Fuse A, Igarashi Y, Tanaka T, et al. Onsite medical rounds and fact-finding activities conducted by Nippon Medical School in Miyagi prefecture after the Great East Japan Earthquake 2011. *J Nihon Med Sch* 2011;78:401–4.
3. Satoh M, Kikuya M, Ohkubo T, Imai Y. Acute and subacute effects of the great East Japan earthquake on home blood pressure values. *Hypertension* 2011;58:e193–4.
4. Tsuji M, Kanda H, Kakamu T, et al. An assessment of radiation doses at an educational institution 57.8 km away from the Fukushima Daiichi nuclear power plant 1 month after the nuclear accident. *Environ Health Prev Med* 2012;17:124–30.
5. Kanamori H, Kunishima H, Tokuda K, Kaku M. Infection control campaign at evacuation centers in Miyagi prefecture after the Great East Japan Earthquake. *Infect Control Hosp Epidemiol* 2011;32:824–6.
6. Sato M, Ishikawa T, Ujihara N, et al. Displacement above the hypocenter. *Science* 2011;332:1395.
7. Takeda M. Mental health care and East Japan Great Earthquake. *Psychiatry Clin Neurosci* 2011;65:207–12 .
8. Johnston GT. Into the next stage: Sendai quake, tsunami, test Japan's spirit. (First published in The Rafu Shimpo on March 17, 2011.) Available at: http://rafu.com/news/2011/03/itns-3/. Accessed July 18, 2012.
9. Reizenstein P. Carcinogenicity of radiation doses caused by the Chernobyl fall-out in Sweden, and prevention of possible tumors. *Med Oncol Tumor Pharmacother* 1987;4:1–5.
10. Hossono G. Ministry of Environment, 2012. Available at: http://housyasen.taiki.go.jp/. Accessed July 18, 2012.
11. Coggle JE, Lambert BE, Moores SR. Radiation effects in the lung. *Environ Health Perspect* 1986;70:261–91.
12. Zeighami EA, Morris MD. Thyroid cancer risk in the population around the Nevada Test Site. *Health Phys* 1986;50:19–32.